International Journal of Impact Engineering 134 (2019) 103368

Contents lists available at ScienceDirect

International Journal of Impact Engineering

journal homepage: www.elsevier.com/locate/ijimpeng

Novel propagation behavior of impact stress wave in one-dimensional hollow spherical structures

Yin Sha[a,b], Chen Dianhao[a,b], Xu Jun[a,b,*]

[a] Vehicle Energy & Safety Laboratory (VESL), Beihang University, Beijing 100191, China
[b] Department of Automotive Engineering, School of Transportation Science and Engineering, Beihang University, Beijing 100191, China

ARTICLE INFO

Keywords:
One-dimensional chain
Hollow sphere
Highly nonlinear solitary wave
Periodical

ABSTRACT

Solitary wave propagation behavior within a granular crystal chain is fundamentally important for impact wave mitigation. Here, we study the propagation behavior of traveling waves in a one-dimensional (1D) mixed chain of stainless-steel and polytetrafluoroethylene dimer hollow spherical particles. The formation and propagation of a unique, highly nonlinear, solitary wave is observed. To have an in-depth understanding of the wave propagation behavior, we establish numerical theoretical models to describe the wave behavior and agree well with the experiment. We also discover that different configurations of dimer wall thicknesses largely influence not only the nonlinear contact interaction between neighboring spheres but also the physical relation of wave velocity V_s and dynamic force F_m. The influence of different ratios of elastic moduli and densities in a dimer is also studied. Results may shed light on the design and evaluation of the 1D chain for supporting specific wave propagation for possible engineering application.

1. Introduction

Mechanical wave mitigation [1–3], amplification [4], and manipulation [5–7] have been a well-researched topic for decades due to its crucial civil and military applications. Waves propagating in granular crystals have been widely studied for its distinct and tunable properties at various length scales, i.e., macro [8–28], meso [29], and nano scales [30–33]. For example, the solitary wave, which was first predicted and discovered in granular crystals by Nesterenko in the 1980s [34,35], has been found to exist in various one-dimensional (1D) granular systems. These systems can be tuned to exhibit linear, weakly nonlinear, or strongly nonlinear regimes [34,36]. Wave characteristics are largely influenced by material properties, particle size and periodicity [9,14,18,19,24–26]. The granular crystal can potentially be used in a variety of engineering applications, such as acoustic lens [37], shock-absorbing materials [3,38,39], and acoustic switches [40], because of its tunability.

In 1D homogeneous granular chains, the contact interaction between solid particles is usually described by Hertz law, which supports highly nonlinear solitary waves. Hertz interaction is characterized by a nonlinear relation between contact force F and relative displacement δ: $F \sim \delta^{1.5}$. An additional source of nonlinearity is zero tensile strength. If initial precompression is significantly larger than dynamic amplitude of the solitary wave it can be considered as a weakly nonlinear described by the Korteweg–de Vries (KdV) equation [34,36]. This KdV equation was first introduced to describe weakly nonlinear waves on the surface of fluid [41]. On the basis of these results, more research on inhomogeneous granular chains made of various materials, such as periodic (dimer/trimer) and disordered ones [18,20,23,34,36], has been conducted. Hertz law still governs the contact properties and the wave passing through when adjacent particles with different material properties collide with each other elastically.

However, when particles in the 1D chain become hollow, the contact interaction seems to change. Pauchard and Rica studied the contact of elastic, spherical, thin-walled shells with rigid plates under compression and found a new contact relation F–$\delta^{1.2}$ in the experiment [11]. Results implied that the nonlinearity of contact interaction in the thin-walled structures could weaken. Ngo et al. validated this finding by studying the influence of particle wall thickness on solitary waves traveling in 1D granular chains, which comprised uniform hollow spherical balls [14]. As the particle wall thickness changes, the nonlinear exponent in the F–δ relation can vary from ~1.2 to ~1.5 (by comparison, solid particles can be considered a limiting case of hollow particles, whose wall thickness is equal to its radius). Furthermore, the exponent can even be lower than 1 in the contact of hollow elliptical cylinder chains [9]. Interaction law with exponent less than 1 results in completely different behavior of discrete chains [36]. In this case such chains with elastic softening do not support strongly nonlinear

* Corresponding author.
E-mail address: junxu@buaa.edu.cn (J. Xu).

https://doi.org/10.1016/j.ijimpeng.2019.103368
Received 24 June 2019; Received in revised form 6 August 2019; Accepted 9 August 2019
Available online 10 August 2019
0734-743X/

compression Nesterenko solitary waves. Instead they may support strongly nonlinear rarefaction solitary waves with ability to disintegrate impact pulse even without dissipation [42].

Nonlinear dynamic response of homogeneous 1D granular chains comprising solid particles with general contact interaction law different than Hertz contact law was theoretically considered in [36,43,44]. But results related to dimers chain composed from hollow particles and specific properties and their tunability of waves in corresponding chains are not published. Thus, it limits the understanding and wide application of such systems.

Therefore, in this study, we investigate the properties of waves excited by impact in the 1D chain composed of hollow particles with specific contact laws. To understand the tunability of hollow granular 1D systems, we study influence of different properties of particles, which may affect their dynamic response. The rest of this paper is organized as follows: In Section 2, we introduce the experimental setup. In Section 3, we develop a theory based on long-wavelength approximation and obtain some wave properties analytically. In Section 4, we model the contact interaction of dimer hollow particles and the entire impact procedure of the 1D dimer chain using finite element (FE) methods. In Section 5, we compare the experimental, theoretical, and numerical results and discuss the effect of particles with different wall thicknesses, elastic moduli, and densities.

2. Experimental setup

A 1D dimer chain composed of 13 hollow stainless-steel particles and 12 hollow polytetrafluoroethylene (PTFE) particles were placed horizontally on a metal supporting rod, as shown in Fig. 1(a). The rod assured that the motion of hollow spheres was unidirectional along the chain's axis. Each "1:1 dimer" contained one hollow steel bead (304 type) with high modulus and density, which alternated with one PTFE bead with low modulus and density. The stainless-steel spheres had an external diameter D_s of $18.80^{+0.42}_{-0.08}$ mm and wall thickness w_s of 0.37 mm, giving an outer radius R_{so} and inner radius R_{si} of 9.40 and 9.03 mm, respectively. The PTFE beads had an external diameter D_p of $18.80^{-0.03}_{-0.16}$ mm and wall thickness w_p of 1.50 mm, giving an outer radius R_{po} and inner radius R_{pi} of 9.40 and 7.90 mm, respectively.

The force–time curves were acquired by placing three instrumented beads in the 9th, 17th, and 22nd positions of the dimer chain. In the instrumented bead, a lead zirconate titanate (PZT) piezoelectric ring sensor (the outer and inner radii were 9.5 and 6.0 mm, respectively, and the thickness was 0.9 mm), provided by Shouguang Feitian Electronic Co., Ltd., was glued in between two halves of a steel or PTFE sphere and using an epoxy layer [14,16,19] (Fig. 1(b)). The material properties for stainless-steel, PTFE beads, and PZT sensors (PZT-5A) are summarized in Table 1. It should be noticed that the value of elastic modulus of PTFE is related to dynamic contact deformation being significantly different from the static value.

The ultrafine lines soldered on the two sides of the sensor were connected to an oscilloscope (Tektronix TDS 2024C), which could acquire waves of dynamic forces and calculate the wave speed in the chain. Three piezoelectric sensors were calibrated using a high-precision (the relative error was under 3‰) calibrated silicon crystal piezoelectric sensor provided by Ketu Electronic Co., Ltd. (Supplementary Material) Hollow stainless-steel strikers from different heights of a ramp were launched to collide with the chain to obtain traveling waves. The striker was identical to hollow steel balls in the chain, and its velocity was measured using a photoelectric timer. Furthermore, the entire process of impact in a single experiment was captured by a high-speed camera to calculate the speed precisely (Fig. S2).

Table 1
Material properties (mass, elastic modulus E, and Poisson's ratio ν) for stainless steel, PTFE, and PZT-5A. The value of the Young's modulus of the PTFE bead and the properties of the PZT sensors were measured and offered by suppliers. And The Poisson's ratio of PTFE is employed from Ref. [16].

Material	Mass (g)	E (GPa)	ν
Steel [12,20]	2.97	193	0.3
PTFE [16]	2.91	1.14	0.46
PZT-5A	1.19	74	0.36

3. Theoretical analysis

We introduce a power law contact force with a general contact index n (Hertz contact is a specific situation of the power law contact when $n = 3/2$) and an arbitrary mass ratio of the rescaled equations of motion [20,36]:

$$m_1\ddot{u}_j = (w_j - u_j)^n - (u_j - w_{j-1})^n, \tag{1}$$

$$m_2\ddot{w}_j = (u_{j+1} - w_j)^n - (w_j - u_j)^n, \tag{2}$$

where u_j (w_j) represents the displacement of the jth stainless-steel (PTFE) particles with a mass of m_1 (m_2).

The distance from u_j to w_j (from u_j to u_{j+1}) is D ($2D$). The small parameter D is compared with the wave spatial range; thus, a long-wavelength approximation (LWA) is used by the Taylor expansion of Eqs. (1) and (2) in which we regard u and w as continuous functions. Furthermore, a consistency condition is introduced following [45] to decouple and "homogenize" the two equations:

$$w = \lambda(u + b_1 D u_x + b_2 D^2 u_{xx} + b_3 D^3 u_{xxx} + b_4 D^4 u_{4x} + \cdots) \tag{3}$$

in which two values for parameter λ exist according to the continuum approximation: 1 and $-m_1/m_2$ corresponding to acoustic excitations and optical ones, respectively. Here, we study the case of $\lambda = 1$ in the subsequent derivation because the excitation applied on the dimer chain is similar to [19,20]. After neglecting high-order terms in Eq. (3), we retain the expanded PDEs for two mass types, which are identical at orders D^n–D^{n+3}. Then, we obtain the demand for the values of b_i ($i = 1,2,3,4$):

$$b_1 = 1, \tag{4}$$

$$b_2 = \frac{m_1}{m_1 + m_2}, \tag{5}$$

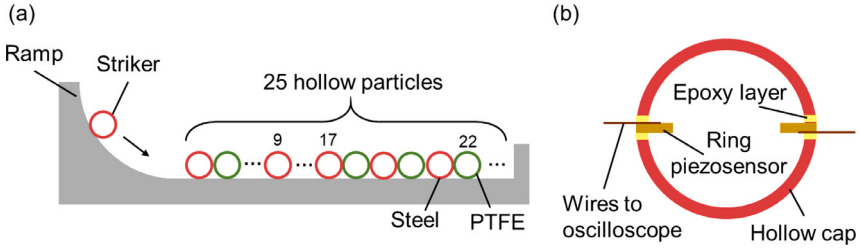

Fig. 1. (a) Experimental setup for a hollow chain consisting of 1:1 dimers of steel:PTFE particles; The propagating waves were obtained at particles 9, 17, and 22. (b) Schematic of a hollow particle with an embedded ring piezoelectric sensor.

$$b_3 = \frac{2m_1 - m_2}{3(m_1 + m_2)}, \tag{6}$$

$$b_4 = \frac{m_1(m_1^2 - m_1 m_2 + m_2^2)}{3(m_1 + m_2)^3}. \tag{7}$$

For a homogeneous chain ($m_1 = m_2$), Eq. (3) with a corresponding b_i becomes a Taylor expansion of w in the neighborhood (D) of u, which transforms to Nesterenko's theory of homogeneous discrete materials [36]. Substituting b_i into the result of the expanded equations of motion, we obtain a "homogenized" PDE:

$$u_{\tau\tau} = u_x^{n-1}u_{xx} + Gu_x^{n-3}u_{xx}^3 + Hu_x^{n-2}u_{xx}u_{xxx} + Iu_x^{n-1}u_{4x}, \tag{8}$$

where $\tau = t\sqrt{2nD^{n+1}/(m_1 + m_2)}$ is a rescaled time, and coefficients in Eq. (8) are as follows:

$$G = D^2\frac{(2 - 3n + n^2)m_1^2}{6(m_1 + m_2)^2}, \tag{9}$$

$$H = D^2\frac{(n-1)(2m_1 - m_2)}{3(m_1 + m_2)}, \tag{10}$$

$$I = D^2\frac{(m_1^2 - m_1 m_2 + m_2^2)}{3(m_1 + m_2)^2}. \tag{11}$$

We should find the traveling wave solutions $u \equiv u(\xi)$ for the PDE of the 1D dimer chain in our experiments, where $\xi = x - V_s\tau$ with the (renormalized) wave speed $V_s = dx/d\tau$. We obtain an ordinary differential equation (ODE) for $u_\xi = v$ (reduce Eq. (8) to three orders). Following the mathematical methods in [20], we convert the ODE into a tractable one, $z_{\xi\xi} = \mu z^\eta - \sigma z$, where $\mu = V_s^2/[I(p + a)]$, $\eta = 1 + p(1 - n)$, and $\sigma = 1/[I(np + a)]$. Finally, we integrate the equation and obtain:

$$u_\xi \equiv v \equiv z^p = B\cos^{\frac{2}{n-1}}(\beta\xi), \tag{12}$$

where $B = (\mu/[\beta^2 s(s-1)])^{1/(n-1)}$, $\beta = \sqrt{\sigma}(1 - \eta)/2$, and $s = 2/(1 - \eta)$ (Similar to [36]).

Therefore, the trigonometric solution based on LWA is valid for the dynamic study of a granular chain consisting of solid beads [19,20].

A power law is used with different n to demonstrate the elastic contact of hollow beads; thus, the theory with a general contact coefficient n may be extended to describe waves passing through a heterogeneous chain of hollow balls. To validate this assumption, we select two properties in the solution, i.e., the amplitude–velocity scaling $B \sim V_s^{2/(n-1)}$ and the solution width π/β, which is controlled directly by the value of mass ratio. For Hertz contact ($n = 3/2$), the range of pulses will be approximately 5 sites under the condition of $m_1 = m_2$ (previously known in [36]). It is worth noting that analytical solutions for solitary waves in the homogeneous chain with power law interaction were available in Ref. [36], which can be divided into two kinds: rarefaction solitary waves ($n < 1$) and compression solitary waves ($n > 1$). The former kind presents an anomalous strain softening behavior [42] and the latter one can be seen as a special case in previous analysis when $m_1 = m_2$.

4. Numerical simulation

4.1. Contact interaction between dimer hollow particles

Here, a dimer geometry model consisting of two hemisphere shells is established in Abaqus/CAE (Fig. 2(a)). The material properties (density ρ, elastic modulus E, and Possion's ratio ν) come from Table 1. The interaction of two shells is set as surface-to-surface hard contact to simulate the contact procedure of compression. We use modified quadratic tetrahedron elements (C3D10M) to mesh the shells.

A power law interaction is used to demonstrate the elastic contact between hollow particles:

$$F = A\delta^n, \tag{13}$$

where F is the contact force between adjacent particles; A is the contact stiffness; δ is the approaching displacement of the centers of two adjacent particles; and n is the contact index, which represents the nonlinearity of the 1D chain system.

The contact force–displacement result of the FE dimer model in Fig. 2(b) reveals an index of 1.4, which differs from the values $n = 1.5$ acquired from Hertz contact law, i.e., $F = A\delta^{3/2}$.

4.2. Dynamic impact of the dimer chain

A computational model is established consisting of 13 hollow stainless-steel particles alternated with 12 PTFE ones, as well as a steel striker identical to steel balls in the chain (Fig. 3(a)). Considering that the mass of piezoelectric sensors (1.19 g) are comparable to that of the hollow balls (i.e., steel (2.97 g) and PTFE (2.91 g)), they are also added into the model. Then, an FE simulation of the entire impact process of the 1D dimer chain is performed. The material properties are kept the same as particles used in the experiments. The contact relation between adjacent balls is set as surface-to-surface hard contact with small slides. Gradient meshes are created to guarantee the precision of results and save the computation in which the contact regions of neighboring beads hold the maximum mesh density (Fig. 3(b)). To obtain an appropriate varied grid density, we conduct mesh convergence analysis before impact simulation (Fig. 3(c)), and the mesh size of 0.10–2 mm is selected. No dissipation is considered during the simulation of ball impact.

5. Results and discussion

5.1. Results of experiments, theory, and numerical simulations

Under the configuration of the dimer chain used in experiments, the dynamic force curves were obtained by sensors when the striker was released from ramp heights of nearly 0–10 cm for impact with the 1D steel:PTFE dimer chain. Fig. 4(a) shows the curves measured through sensors in the 9th, 17th, and 22nd balls when the velocity of the striker is 0.59 m/s. The one-hump waveform indicates that solitary waves spread through the whole chain. The wave speed in the corresponding condition is 147 m/s, which was calculated using the time-of-flight measurements. And the amplitude of dynamic force F_m is obtained by averaging the amplitudes of the corresponding forces measured in the 9th ($F_{9\mathrm{m}}$) and 22nd ($F_{22\mathrm{m}}$) balls, i.e., $F_m = (F_{9m} + F_{22m})/2$. The curve of the amplitude of dynamic force (F_m) and the wave velocity (V_s) is almost linear in a logarithmic relationship (Fig. 5(a)), which gives a slope of 0.152. Moreover, the average wave width from tail to tail is approximately 5.7 sites in the experiments. During the impact experiments, the motions of the particles in the dimer chain captured by a high-speed camera displayed a light rotation of spheres along the axis of the guide rail (Fig. S2 and Movie S1), which may have influenced the waves measured by the sensors when the velocity of striker was high.

In Section 3, a theoretical analysis based on LWA is developed and gives the relation $F_m \sim B^n \sim V_s^{2n/(n-1)}$. This relation yields $V_s \sim F_m^{0.167}$ when the steel:PTFE dimer chain is made of solid particles or when the chain is homogenous ($n = 3/2$). By contrast, the relation becomes $V_s \sim F_m^{0.141}$, where the contact index of the dimer is obtained in Section 4 ($n = 1.4$). In addition, the exponent $n = 1.4$ calculated in the simulation of contact interaction gives the theoretical value of the wave width, which is approximately 6 sites. It should be noticed that the F_m–V_s relation mentioned above is similar to Eq. 1.129 in [36] if the maximum force is replaced by maximum relative displacement. And the length of solitary wave depending on the contact index can be calculated by Eq.1.130 in [36] as long as $m_1 = m_2$.

The corresponding wave figures of dynamic forces in FE simulations (Fig. 4(b)) are acquired by averaging the contact forces of the two sides of instrumented beads on each time step (Fig. 2 in [16]). FE results

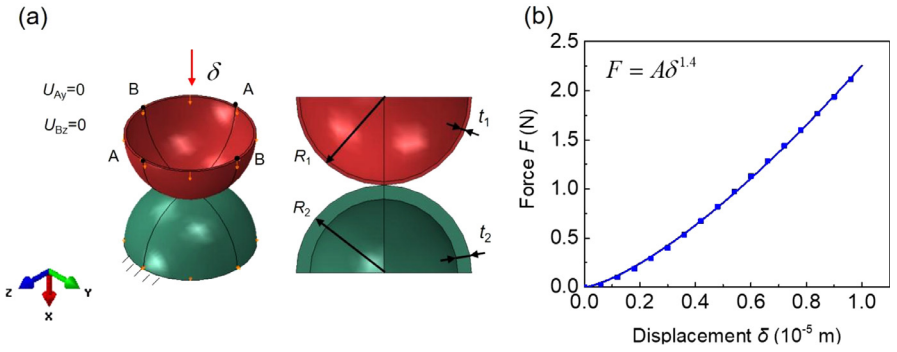

Fig. 2. (a) Diagram of the boundary conditions of a 1:1 dimer FE model. The red shell represents a steel hemisphere, whereas the green one represents a PTFE hemisphere; (b) Contact interaction obtained from the FE dimer model in which the thicknesses of stainless-steel (t_1) and PTFE (t_2) particles are 0.36 and 1.49 mm, respectively, which corresponds to the experimental setup. The dots represent the FE result and the solid line is a fitting curve of it.(For interpretation of the references to colour in this figure legend, the reader is referred to the web version of this article.)

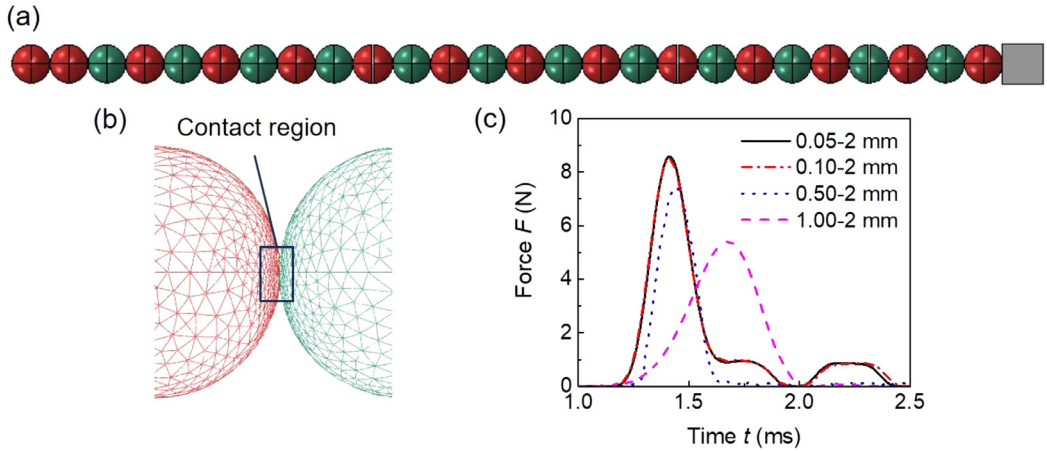

Fig. 3. FE simulation of 1D hollow 1:1 steel:PTFE dimer chain. (a) FE model of the entire granular chain. The red balls represent stainless-steel particles, whereas the green ones represent PTFE particles; (b) Meshing results of the contact region between hollow dimer particles; (c) Graph of dynamic forces acquired from the FE models with different mesh sizes. The dynamic force is obtained by averaging the contact forces on two sides of a particle (Here is the 15th bead) in the dimer chain. (For interpretation of the references to colour in this figure legend, the reader is referred to the web version of this article.)

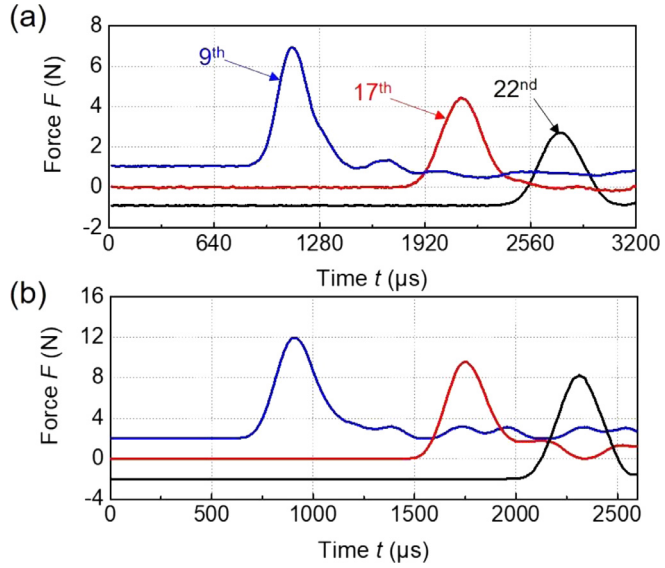

Fig. 4. Solitary waves in the 1:1 steel:PTFE dimer chain generated by a hollow stainless- steel striker with a velocity of 0.59 m/s. The initial values of the force curves are adjusted manually just for a better visual distinction. (a) Incident solitary waves captured experimentally in the dimer chain of hollow beads with an outer diameter of 18.8 mm. The numbered arrows point to the corresponding particles in the chain. The third curve (obtained from particle 22) represents results from a PTFE bead, and the other curves represent those from steel beads. (b) FE results for a discrete chain under conditions that are identical to those in (a). The curves represent the average forces acting on the two sides of each sensor.

reveal a solitary wave speed of 180 m/s. The average wave width is approximately 5 sites.

The experimental solitary waves and V_s–F_m curves agree well with those of the FE simulation, although a dissipation in the experimental results of force amplitudes corresponding to FE results is observed (Figs. 4 and 5). Comparing the V_s–F_m relation from theory and experiments, data measured from the experiments show an exponential relation yielding $V_s \sim F_m^{0.152}$ in which the power is very close to the theory-predicted value of 0.141. This relation is also validated via FE simulation (Fig. 5(a)). The deviation of force amplitudes is mainly caused by oscilloscope noise and sensor misalignment. Such deviation will be clearly visible at low-impact speed. Meanwhile, sensor misalignment can incline the entire wave shape, thereby reducing the amplitudes of forces and altering the exact peak time.

Fig. 5(b) also shows good agreement among experiments, theory, and FE simulations. The wave width in a dimer chain is larger than the width of a solitary wave in a homogenous chain ($m_1 = m_2$, 5 sites). This result can be explained by the "homogenized" theory in the previous section. The wave widths of steel and PTFE particles in dimers exhibit a small gap for the different materials used in adjacent balls. As the wave propagates through the chain, the shape of solitary wave forms from a pulse with high amplitude and stabilizes after passing through approximately nine balls. This occurrence can be observed from the change of the guide line fluctuation in Fig. 5(b).

5.2. Wall thicknesses of the dimer

FE simulations of models with various configurations of dimer thicknesses are conducted because previous research has shown that the thicknesses of hollow particles can determine the properties of

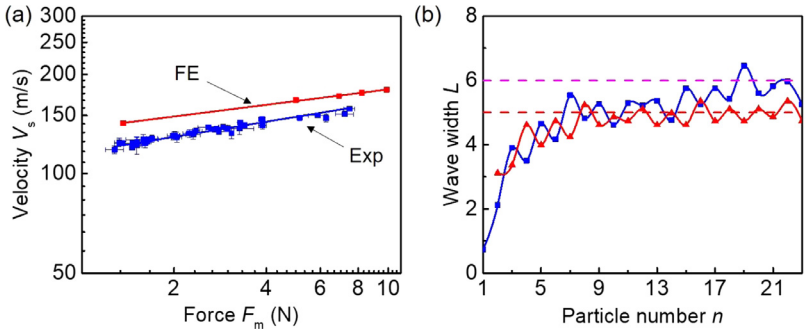

Fig. 5. Comparison of experiments, theory, and FE simulations. (a) Dependence of wave propagating velocity on dynamic force amplitude in a 1:1 steel:PTFE dimer chain. The solid lines represent the fitting curves of experimental and FE results; (b) Evolution of solitary wave width with particle number. The experimental and FE simulation values are represented by solid squares and solid triangles, respectively (We use curves to connect the dots as visual guides). The pink dotted line represents the theoretical wave width, and the red one represents the result of homogeneous chain.(For interpretation of the references to colour in this figure legend, the reader is referred to the web version of this article.)

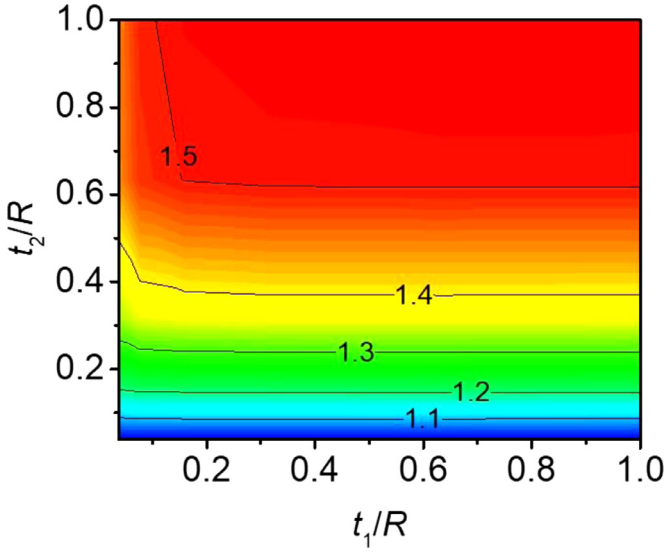

Fig. 6. Contact index as a function of the normalized wall thicknesses of steel (t_1/R) and PTFE (t_2/R) balls. The outer radius of the hollow particle R (9.4 mm) is a constant.

waves propagating in the chain. As shown in Fig. 6, these configurations largely influence the nonlinearity of the dimer's contact, which can be reflected from the change of contact index, whose value n depends on t_1/R and t_2/R, calculated by fitting the curves of the FE simulation based on the power law of contact.

Results show that the level of influence that a PTFE particle has on the contact interaction is quite different from a steel particle, considering the wall thickness. When the (normalized) thickness of steel balls t_1/R is larger than approximately 0.16, the nonlinearity is completely controlled by the PTFE ball of which the index increases from approximately 1.0 (nearly linear) to 1.5 (highly nonlinear) as the hollow ball becomes thicker. When t_1/R is smaller than 0.16, the influence of the wall thickness of the steel ball shows a limited effect and becomes evident as the PTFE ball's wall thickness increases. This kind of difference is mainly due to the distinct elastic properties of these two materials. The change of wall thicknesses of “hard” (steel) or “soft” (PTFE) particles affects the local elastic deformation of particles to varying degrees. When the wall thickness of “hard” particles is very thin, the deformation in the contact region will be complex under impact, and nonlinearity is simultaneously reduced. This situation disappears rapidly when the wall thickness increases. On the contrary, the deformation of “soft” particles is quite larger than that of the “hard” ones, mainly contributing to the relative displacement of adjacent particles. Therefore, the properties of propagating waves largely depend on the wall thickness of PTFE balls.

To study the link between wave properties and particle wall thickness, we select some specific dimer configurations (Fig. 7). The contact force increases rapidly because the stiffness and nonlinearity of contact rise with the increase in particle wall thickness (Fig. 7(a)). Consequently, the different relations of solitary wave velocity (V_s), which

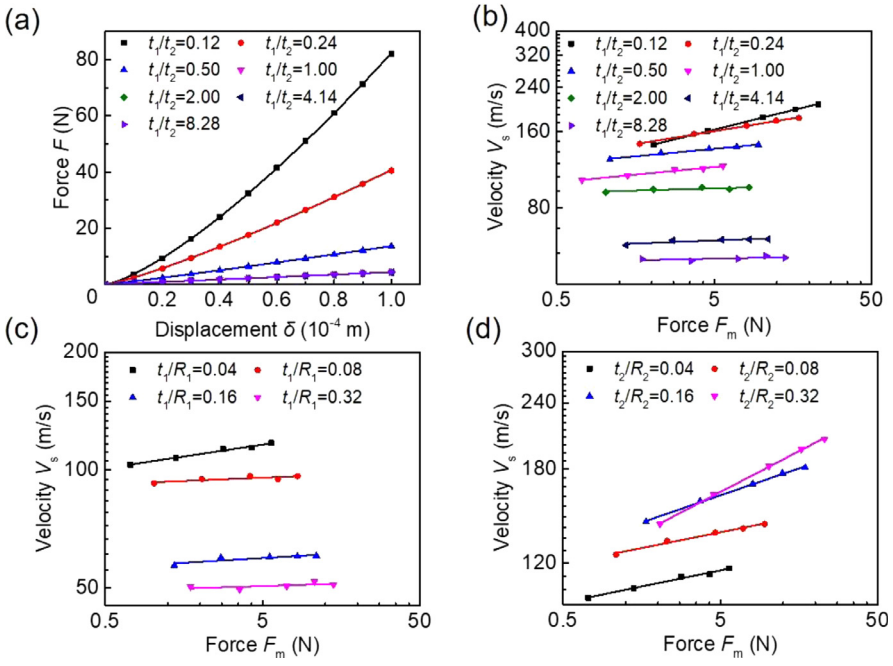

Fig. 7. Contact and wave propagating properties of 1D chains with different thickness ratios of steel:PTFE dimers acquired from FE simulations. (a) Contact interactions for selected values of thickness ratios; (b) Relations between contact force and propagating velocity under different thickness ratios; (c) and (d) show that the wave speed varies with maximum dynamic force under different thicknesses of hollow steel (t_1) and hollow PTFE (t_2) balls, respectively. Their radii (R_1 and R_2) are equal to 9.4 mm. The solid lines represent the fitting curves of FE results (solid dots).

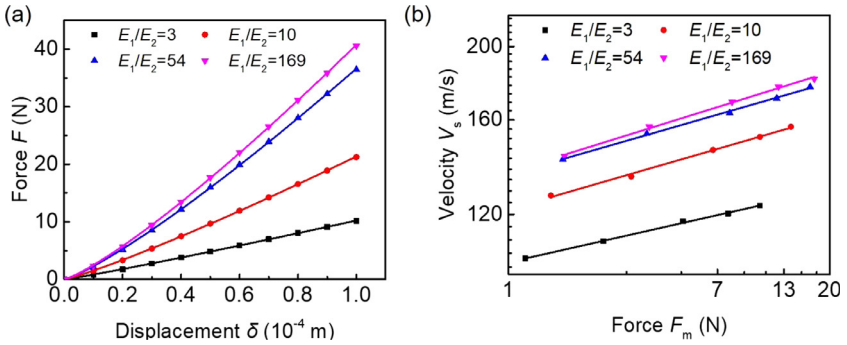

Fig. 8. Contact and wave propagating properties of the chains with different elastic modulus ratios of 1:1 dimer acquired from FE simulations ($E_2 \equiv 1.14$ GPa). (a) Contact interactions for specific values of elastic modulus ratio; (b) Relation between contact force and propagating velocity under different density ratios. The dots represent FE results, and the solid lines represent the fitting curves of the corresponding results.

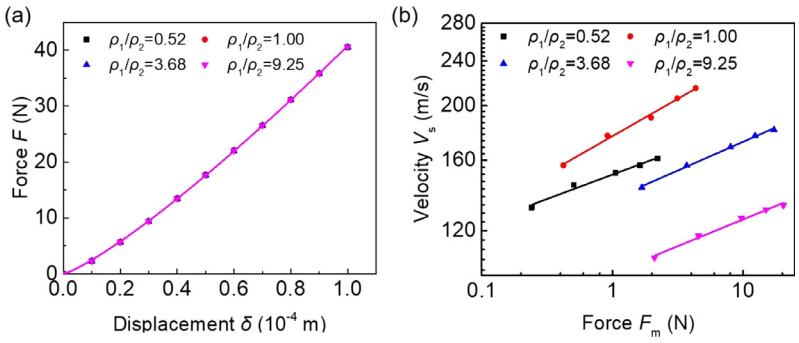

Fig. 9. Contact and propagating wave properties of the chains with different density ratios of 1:1 dimer acquired from FE simulations ($\rho_2 \equiv 2086$ kg/m^3). (a) Contact interactions for specific values of density ratio; (b) Relations between contact force and propagating velocity under different density ratios. The dots represent FE results, and the solid lines represent the fitting curves of the corresponding results.

depend on the dynamic force amplitude (F_m) under selected t_1/t_2 configurations, become distinct (Fig. 7(b)). When the value of t_1/t_2 varies from 0.12 to 1.00, the solitary wave speed and growth rate decrease with the increase in dynamic force. This relationship is directly indicated from the slopes of the fitted solid lines. When $t_1/t_2 > 1.00$, the fitting curves are almost horizontal, indicating that similar to that of the KdV solitary wave, the wave speed will remain the same regardless of how the dynamic force changes in the range in this study. The wave speed can decrease (nearly 50 m/s) as t_1/t_2 increases. Fig. 7(c) and (d) show the Vs–F_m relations under different wall thicknesses of steel (PTFE) spheres. As the wall thickness of steel particles increases, solitary wave velocity and nonlinearity decrease. However, when the wall thickness of PTFE particles increases, the corresponding wave speed and nonlinearity increase. The different results of the increase in the wall thicknesses of steel and PTFE beads can be used to adjust the solitary wave speed.

5.3. Elastic modulus of the dimer

The influence of the elastic modulus ratio of a dimer (E_1/E_2) on wave properties is shown in Fig. 8. When the moduli of two kinds of materials used in a dimer are close to each other, the contact interaction is nearly linear. As the ratio increases, the contact force increases rapidly because of the rise of its stiffness and index (Fig. 8(a)). Increasing the ratio of elastic modulus also contributes to the nonlinear contact of dimers. This kind of mismatch creates a “hard” and a “soft” particle in a dimer, between which a nonlinear contact exists. The enhance of this mismatch causes an increase in nonlinearity. Nevertheless, the change of contact interaction becomes much smaller when the ratio of modulus increases, which can be derived from the difference between adjacent curves. This result indicates that the control of the ratio of elastic modulus is limited.

The V_s–F_m relations are also shown in Fig. 8(b). The entire level of wave velocity increases with the increase in modulus ratio. Thus, a high but limited wave speed can be achieved by increasing the modulus mismatch. This relation can be attributed to an increase in the stiffness of the entire granular chain and results in less-deformed contact regions in particles, thus causing the traveling wave to pass through the chain quickly.

5.4. Density of the dimer

The contact and wave properties of dimer chains with different density ratios of particles are shown in Fig. 9. The nonlinear contact interaction is entirely unchanged when the ratio of density varies (Fig. 9(a)). The density of particles has no effect on the local deformation in the contact region between adjacent particles. Thus, the nonlinearity of the granular system remains nearly the same.

Meanwhile, the wave velocity changes as the ratio of density increases. When the ratio of density increases to 1.00, the level of wave velocity seems to climb to the largest value and then decline afterward, indicating that close values of density of the two kinds of beads in a dimer lead to a high wave velocity to some extent.

6. Conclusion

The propagation of solitary waves in 1D 1:1 steel:PTFE dimer chain of hollow spherical particles is investigated using systematic experimental, FE simulation, and theoretical methods. Compared with the Hertz contact between solid particles ($n = 3/2$), a power law type interaction can demonstrate the contact between hollow particles more exactly. The nonlinearity of the system can be tuned from a nearly linear to strongly nonlinear regime by controlling the wall thicknesses and the ratio of elastic modulus in a dimer, and the relation of wave velocity V_s and dynamic force F_m varies accordingly. The wave properties (V_s–F_m relation) can also be influenced by the ratio of density. These findings offer some controlling factors to tune the wave properties in a granular crystal and the patterns of change. Results may lay a solid foundation for the understanding of wave behaviors in lightweight, hollow-structured chains and provide useful guidance for engineering design.

Acknowledgements

This work was financially supported by the National Key Research and Development Program of China (2017YFB0103703), the

Fundamental Research Funds for the Central Universities, Beihang University and Young Elite Scientist Sponsorship Program by CAST.

Supplementary materials

Supplementary material associated with this article can be found, in the online version, at doi:10.1016/j.ijimpeng.2019.103368.

References

[1] Fraternali F, Porter MA, Daraio C. Optimal design of composite granular protectors. Mech Adv Mater Struct 2009;17:1–19.
[2] Carretero-Gonzalez R, Khatri D, Porter MA, Kevrekidis PG, Daraio C. Dissipative solitary waves in granular crystals. Phys Rev Lett 2009;102:024102.
[3] Kim E, Yang J, Hwang H, Shul CW. Impact and blast mitigation using locally resonant woodpile metamaterials. Int J Impact Eng 2017;101:24–31.
[4] Choon Mahn P, Jong Jin P, Seung Hwan L, Mun SY, Chul Koo K, Lee SH. Amplification of acoustic evanescent waves using metamaterial slabs. Phys Rev Lett 2011;107:194301.
[5] Chaunsali R, Toles M, Yang J, Kim E. Extreme control of impulse transmission by cylinder-based nonlinear phononic crystals. J Mech Phys Solids 2017;107:21–32.
[6] Jiang S, Shen L, Guillard F, Einav I. Energy dissipation from two-glass-bead chains under impact. Int J Impact Eng 2018;114:160–8.
[7] Du Y, Wang S, Zhang J. Energy dissipation in collision of two balls covered by fine particles. Int J Impact Eng 2010;37:309–16.
[8] Herbold EB, Kim J, Nesterenko VF, Wang SY, Daraio C. Pulse propagation in a linear and nonlinear diatomic periodic chain: effects of acoustic frequency band-gap. Acta Mech 2009;205:85–103.
[9] Kim H, Kim E, Chong C, Kevrekidis PG, Yang J. Demonstration of dispersive rarefaction shocks in hollow elliptical cylinder chains. Phys Rev Lett 2018;120:194101.
[10] Hertz H. On the contact of rigid elastic solids. J Reine Angew Math 1881;92:156–71.
[11] Pauchard L, Rica S. Contact and compression of elastic spherical shells: the physics of a 'ping-pong' ball. Phil Mag Part B 1998;78:225–33.
[12] Updike DP, Kalnins A. Axisymmetric behavior of an elastic spherical shell compressed between rigid plates. J Appl Mech 1970;37:635.
[13] Updlike DP, Kalnins A. Axisymmetric postbuckling and nonsymmetric buckling of a spherical shell compressed between rigid plates. J Appl Mech 1972;39:172–8.
[14] Ngo D, Griffiths S, Khatri D, Daraio C. Highly nonlinear solitary waves in chains of hollow spherical particles. Granul Matter 2013;15:149–55.
[15] Daraio C, Nesterenko VF, Herbold EB, Jin S. Tunability of solitary wave properties in one-dimensional strongly nonlinear phononic crystals. Phys Rev E 2006;73:026610.
[16] Daraio C, Nesterenko VF, Herbold EB, Jin S. Strongly nonlinear waves in a chain of Teflon beads. Phys Rev E 2005;72:016603.
[17] Daraio C, Nesterenko VF. Strongly nonlinear wave dynamics in a chain of polymer coated beads. Phys Rev E Stat Nonlinear Soft Matter Phys 2006;73:026612.
[18] Ponson L, Boechler N, Lai YM, Porter MA, Kevrekidis PG, Daraio C. Nonlinear waves in disordered diatomic granular chains. Phys Rev E 2010;82:021301.
[19] Porter MA, Daraio C, Herbold EB, Szelengowicz I, Kevrekidis PG. Highly nonlinear solitary waves in periodic dimer granular chains. Phys Rev E 2008;77:015601.
[20] Porter MA, Daraio C, Szelengowicz I, Herbold EB, Kevrekidis PG. Highly nonlinear solitary waves in heterogeneous periodic granular media. Physica D 2009;238:666–76.
[21] Ngo D, Khatri D, Daraio C. Highly nonlinear solitary waves in chains of ellipsoidal particles. Phys Rev E 2011;84:026610.
[22] Khatri D, Ngo D, Daraio C. Highly nonlinear solitary waves in chains of cylindrical particles. Granul Matter 2011;14:63–9.
[23] Daraio C, Nesterenko VF, Herbold EB, Jin S. Energy trapping and shock disintegration in a composite granular medium. Phys Rev Lett 2006;96:058002.
[24] Nesterenko VF, Daraio C, Herbold EB, Jin S. Anomalous wave reflection at the interface of two strongly nonlinear granular media. Phys Rev Lett 2005;95:158702.
[25] Avagyan A, Chiao D, Dostart N, Zhu K, Cho S, Remick K, Vakakis AF, McFarland DM, Kriven WM. Experimental study of embedded and non-embedded ordered granular chains under impulsive excitation. Acta Mech 2016;227:2511–27.
[26] On T, Wang E, Lambros J. Plastic waves in one-dimensional heterogeneous granular chains under impact loading: single intruders and dimer chains. Int J Solids Struct 2015;62:81–90.
[27] Liu D, Shen L, Guillard F, Einav I. Transition failure stress in a chain of brittle elastic beads under impact. Int J Impact Eng 2016;93:222–30.
[28] Dong XL, Gao ZY, Yu TX. Dynamic crushing of thin-walled spheres: an experimental study. Int J Impact Eng 2008;35:717–26.
[29] Lin W-H, Daraio C. Wave propagation in one-dimensional microscopic granular chains. Phys Rev E 2016;94:052907.
[30] Xu J, Zheng BW, Liu YL. Solitary wave in one-dimensional buckyball system at nanoscale. Sci Rep 2016;6:21052.
[31] Xu J, Zheng BW. Quantitative tuning nanoscale solitary waves. Carbon N Y 2017;111:62–6.
[32] Xu J, Zheng B. Highly effective energy dissipation system based on one-dimensionally arrayed short single-walled carbon nanotubes. Extreme Mech Lett 2016;9:336–41.
[33] Zheng B, Xu J. Mechanical wave propagation within nanogold granular crystals. Extreme Mech Lett 2017;15:17–25.
[34] Nesterenko VF. Propagation of nonlinear compression pulses in granular media. J Appl Mech Tech Phys 1984;24:733–43.
[35] Lazaridi AN, Nesterenko VF. Observation of a new type of solitary waves in a one-dimensional granular medium. J Appl Mech Tech Phys 1985;26:405–8.
[36] Nesterenko VF. Dynamics of heterogeneous materials. Springer; 2001.
[37] Donahue CM, Anzel PWJ, Bonanomi L, Keller TA, Daraio C. Experimental realization of a nonlinear acoustic lens with a tunable focus. Appl Phys Lett 2014;104:014103.
[38] Porter MA, Kevrekidis PG, Daraio C. Granular crystals: nonlinear dynamics meets materials engineering. Phys Today 2015;68:44–50.
[39] Tan KT, Huang HH, Sun CT. Blast-wave impact mitigation using negative effective mass density concept of elastic metamaterials. Int J Impact Eng 2014;64:20–9.
[40] Li F, Anzel P, Yang J, Kevrekidis PG, Daraio C. Granular acoustic switches and logic elements. Nat Commun 2014;5:5311.
[41] Korteweg DJ, De Vries G. XLI. on the change of form of long waves advancing in a rectangular canal, and on a new type of long stationary waves. Lond Edinb Dubl Phil Mag J Sci 1895;39:422–43.
[42] Herbold EB, Nesterenko VF. Propagation of rarefaction pulses in discrete materials with strain-softening behavior. Phys Rev Lett 2013;110:144101.
[43] Nesterenko VF. Waves in strongly nonlinear discrete systems. Phil Trans R Soc A Math Phys Eng Sci 2018;376:20170130.
[44] Sergyeyev A, Skurativskyi S, Vladimirov V. Compacton solutions and (non)integrability of nonlinear evolutionary PDEs associated with a chain of prestressed granules. Nonlinear Anal Real World Appl 2019;47:68–84.
[45] Pnevmatikos S, Flytzanis N, Remoissenet M. Soliton dynamics of nonlinear diatomic lattices. Phys Rev B 1986;33:2308–21.